RSC Advances

ROYAL SOCIETY OF CHEMISTRY

www.rsc.org/advances

Table of Contents

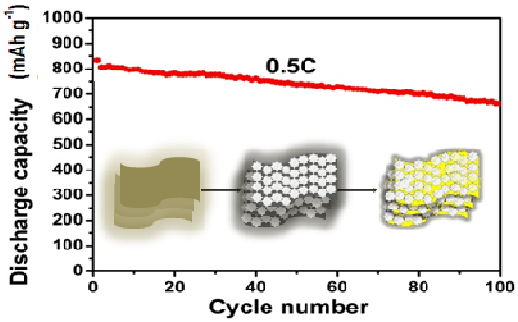

Highlight: The novel structure of ZrO_2@RGO composite provide a layered porous framework for sulfur cathode.

Cite this: DOI: 10.1039/c0xx00000x

www.rsc.org/xxxxxx

ARTICLE TYPE

A Layered porous ZrO_2/RGO composite as sulfur host for Lithium-Sulfur batteries

Chunying Wan, Wangliang Wu, Chuxin Wu, Jiaoxing Xu and Lunhui Guan[a,b*]

Received (in XXX, XXX) Xth XXXXXXXXX 200X, Accepted Xth XXXXXXXXX 200X

DOI: 10.1039/b000000x

A new layered porous nanostructure with ZrO_2 nanoparticles attached on the reduced graphene oxide (ZrO_2/RGO) was synthesized by a facile solvothermal process. The resulting ZrO_2/RGO composite with well-designed mesoporous structure and excellent conductivity not only served as scaffold to house sulfur but also as polysulfide reservoir for lithium-sulfur batteries. This nanostructured S@ZrO_2/RGO electrode exhibits enhanced cycling stability, high specific capacity, and superior coulombic efficiency.

Lithium-sulfur (Li-S) battery is considered as one of the most promising rechargeable battery system, as it possesses an impressive theoretical energy density of about 2600 Wh kg^{-1}, calculated on the basis of the Li anode (3860 mAh g^{-1}) and the S cathode (1675 mAh g^{-1}).[1] What's more, the natural abundance, low cost, and environmental benignity of sulfur make it favorable for future large-scale practical applications.[2] However, the commercialization of the lithium-sulfur battery has been so far hindered by two main problems: ⅰ) the insulating nature of both the sulfur and its solid discharge products (Li_2S and Li_2S_2) result in poor electrode rechargeability and limited rate capability ; ⅱ) long-chain lithium polysulfide (Li_2S_n, 2<n<8) of the intermediate products are soluble in the organic electrolyte. Those intermediate products, shuttling back and forth between the cathode and the anode during the cyclic process, lead to a relatively low coulombic efficiency and poor cycling performance.[3-4]

Enormous efforts, engaged on addressing these issues for the last few years, have mainly focused on designing porous composite as conductive host for sulfur impregnation and polysulfide entrapment, such as porous carbons[5-7] and conducting polymers.[8] Moreover, porous carbons have been regarded as the best host material as they are highly effective in improving both the conductivity of the overall cathode and the adsorption ability.[9] Nevertheless, the diffusion of the polysulfide anions in liquid electrolyte can't be effectively suppressed by pristine carbon materials. In order to further improve the cycling stability of Li-S batteries, active materials coupled with protective layers have been reported.[10-13] Among them, inorganic metal oxides are of great attractive for Li-S batteries in terms of their chemical inertness and strong adsorbability for polysulfide.[14-15] Particularly，the integration of oxide/graphene is quite favorable because those inorganic oxides layers have manifest impact on inhibiting the dissolution of the active sulfur, while graphene can ensure a unique electrical conductivity.[16-17]

Jung *et al*.[18] synthesized a mesoporous graphene-silica composite as a supporting material of sulfur. Since the electronic properties of graphene and the dual functions of silica as both a structural building block and an *in situ* polysulfide adsorbing agent, it shows enhanced cycling stability and discharge/charge rate capacity as compared to SAB-15 and CMK-3. However, its overall performance of capacity was relatively low, only 380 mAh g^{-1} after 40 cycles when at current rate of 0.5 C. In this case, the advantage of high capacity of Li-S battery did not present properly.

Zirconium dioxide, an important inorganic oxide, has been extensively studied in many fields because of its rich abundance, chemical stability, and nontoxicity. It has been reported that the application of inactive ZrO_2 layer coating on electrodes modifies electrolyte-electrode interface and inhibits the reaction between electrolyte and the cathode materials, therefore, greatly improved LIB cycling performances.[19-21] Most recently, ZrO_2 dispersion in the polymer electrolyte for Li-S batteries was also reported.[22] The ZrO_2 fillers not only improved the transport properties of the polymer electrolyte but also acted as interfacial stabilizer in Li-S batteries.

Bearing those in mind， we report a layered porous host for the encapsulation of sulfur as cathode for Li-S battery. A thin layer of ZrO_2 nanoparticles uniformly attached on the surface of reduced graphene oxide (RGO), thus formed the ZrO_2/RGO structure. Within this design, the new composite can be a good matrix, the RGO will enhance the electrical conductivity while the porous layer of ZrO_2 added as a stable sorption reagent for polysulfides. As a result of the synergetic effect of RGO sheets and ZrO_2, the cathode shows high specific capacity, stable cyclability, and superior rate capability.

Fig. 1 illustrated the process for preparing nanostructure ZrO_2/RGO composite. It was experimentally realized through a facile solvethermal process. GO could be easily reduced to RGO under the solvethermal treatment, meanwhile ZrO_2 nanoparticles were formed on the RGO sheets.

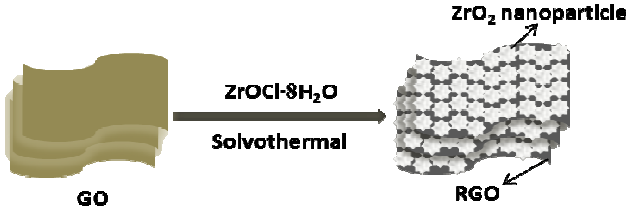

Fig. 1. A schematic shows the preparation of ZrO_2/RGO composite.

The Brunauer-Emmett-Teller (BET) analysis shows that this 2D RGO-based scaffold, decorated with ZrO_2 nanoparticles, gives rise to its specific surface area. The typical IV isotherms and hysteresis loops of the sample **(Fig. 2a)** are characteristic of mesoporous material. The specific surface areas of the samples, calculated by the multipoint BET method, and the single point adsorption total pore volume are listed in Table1. The specific BET surface area of the ZrO_2/RGO sample is 436.20 $m^2 g^{-1}$, and the pore volume is 0.77 cm^3g^{-1}, which are much higher than the pristine RGO and ZrO_2. The increased BET value can be attributed to the synergetic effect between the RGO and the ZrO_2 nanoparticles. On one hand, the RGO sheets serve as substrates for *in situ* formation of ZrO_2 nanoparticals and, on the other, the incorporation of ZrO_2 can effectively prevent the restacking of flexible RGO sheets. After sulfur impregnation **(Fig. S1)**, surface area and pore volume of the obtained S@ZrO_2/RGO composite greatly reduced to 0.18 $m^2 g^{-1}$ and 0.004 cm^3g^{-1}, which implies that the porous structure was effectively occupied with sulfur.

X-ray diffraction (XRD) patterns of pure sulfur, ZrO_2/RGO, and S@ZrO_2/RGO materials are showed in **Fig. 2b**. For the pattern of ZrO_2/RGO, a broad peak appears at 24.5° refers to the success reduction of GO into RGO through a facile solvohermal process. Another two distinct peaks appear at 30.2° and 50.2 ° corresponding to the (011) and (112) diffraction of tetragonal-ZrO_2. The XRD pattern of sulfur matches with that in the literature for *Fddd* orthorhombic sulfur[23]. S@ZrO_2/RGO nanocomposite shows similar but weaker character peaks of sulfur, due to the hybrid nanostructure wrapping.

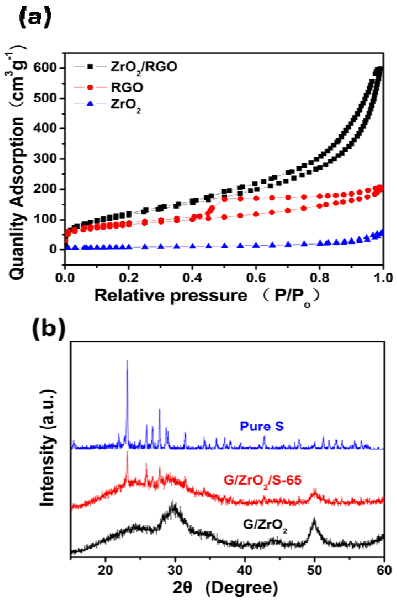

Fig. 2. (a) N_2 adsorption-desorption isotherms of different samples and (b) XRD patterns of ZrO_2/RGO host, S@ZrO_2/RGO composites and pure

Table 1 BET surface areas and BJH pore volumes of different samples.

Sample	BET[m^2g^{-1}]	Total pore volume[cm^3g^{-1}]
RGO	288.80	0.28
ZrO_2	28.28	0.06
ZrO_2/RGO	436.20	0.77

S.

The morphology of the ZrO_2/RGO composite was investigated by filed-emission SEM. As ZrO_2 introduced (**Fig. 3a**), the ZrO_2 nanoparticles are well-decorated on the surface of the flexible RGO without obvious bulk particle observed. ZrO_2/RGO composite was further detailed by TEM. The image in **Fig. 3b** reveals that the RGO is uniformly coated with ZrO_2 nanoparticles, and the magnified TEM image (**Fig. 3c**) clearly shows that the interplanar spacing of 0.29 nm is assigned to the spacing of the (011) planes of ZrO_2.

S@ZrO_2/RGO cathode was prepared by melt-infusion in 155 ℃ under Ar flow. The TGA curve of the S@ZrO_2/RGO composite shows two weight loss stages at around 250 to 320 ℃ and 500 to 650 ℃ (**Fig. S2**). The first loss stage reflects the evaporation of sulfur and the corresponding weight loss is about 65%, corresponds to the TGA result under Ar flow (**Fig. S3**). The second loss stage is ascribed to the combustion of RGO. The content of RGO in the composite is about 16 %, and ZrO_2 is 19%. As shown in the SEM image (**Fig. 3d**), the typical structure of the S@ZrO_2/RGO is similar to the ZrO_2/RGO nanocomposite. After the infusion of sulfur, the surface of S@ZrO_2/RGO composite is smoother than the ZrO_2/RGO. TEM images in **Fig. 3e** and **f** indicate that the sulfur is absorbed into the pore of the ZrO_2/RGO and on the surface. Furthermore, elemental mapping images (**Fig. S4**) show that spatial distributions of C, S, and Zr are highly matched for each other, indicating sulfur is uniformly absorbed by the ZrO_2/RGO host.

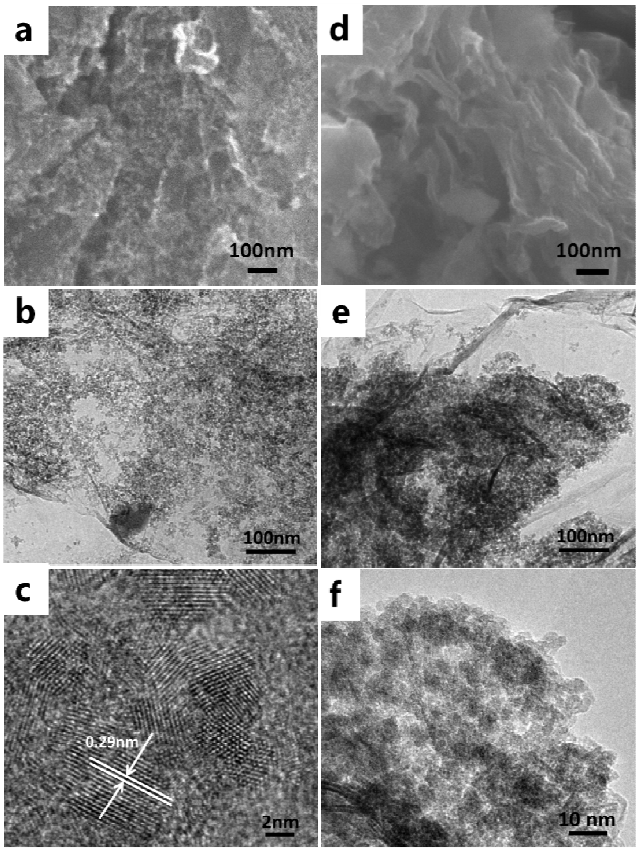

Fig.3. (a) SEM image and (b), (c) TEM images of the ZrO_2/RGO composite; (d) SEM image and (e), (f) TEM images of S@ ZrO_2/RGO composite.

Cyclic voltammetry (CV) curves of the S@ZrO_2/RGO cathode were characterized at a scan rate of 0.2 mV s^{-1}, with potential ranged from 1.5 V to 3.0 V. The CV patterns (**Fig. 4a**) reveal two reduction peaks and one oxidation peak due to the multistep reaction mechanism between sulfur and lithium. The first reduction peak at ~2.35 V corresponds to the conversion of sulfur (S_8) to high order lithium polysulfide (Li_2S_n, $4 \leqslant n \leqslant 8$). And the second reduction peak at ~2.0 V is attributed to the further reduction of long chain lithium polysulfide to Li_2S_2 and finally Li_2S. The oxidation of Li_2S to lithium polysulfide begins at 2.45 V, which is related to the reverse process. The cell exhibits rather stable profiles, revealing good reversibility of the S@ZrO_2/RGO cathode. These results verify that the as-synthesized ZrO_2/RGO nanocomposite is a promising scaffold for high-performance Li-S cathode. **Fig. 4b** demonstrates the galvanostatic charge-discharge voltage profiles of the S@ZrO_2/RGO composite electrode, evaluated at a current density of 0.5 C. All the discharge profiles contain two typical plateaus that correspond to the peaks in the CV curves.

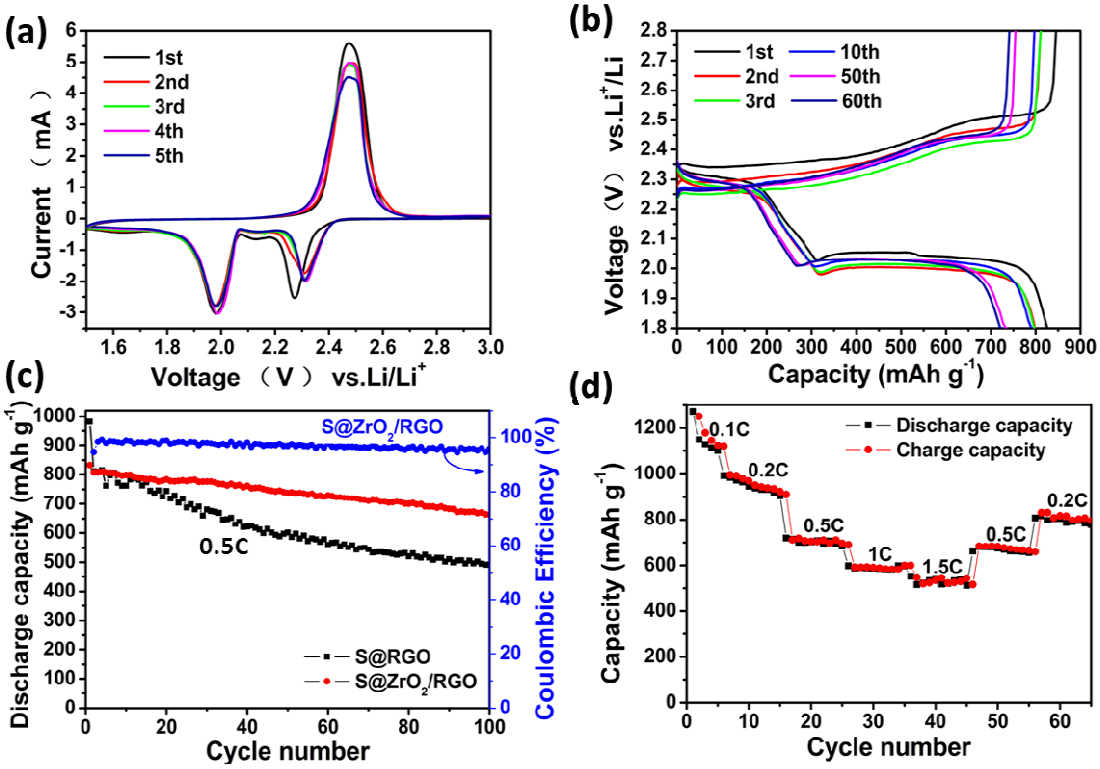

Fig. 4. (a) CV cures of S@ZrO_2/RGO cathode at a scant rate of 0.2 mV s^{-1}; (b) Galvanostatic charge-discharge profiles of S@ZrO_2/RGO cathode at a curent rate of 0.5 C; (c) Cycling prformance at a current rate of 0.5 C of S@ZrO_2/RGO and S@RGO cathodes; (d) Rate capability of the S@ZrO_2/RGO cathode with current densities ranging from 0.1 C to 1.5 C.

In order to clarify the role of ZrO_2 incorporation, a S@RGO composite was also prepared for comparison. As shown in the **Fig. S3,** the sulfur loading of S@RGO composite is 66%, very similar to the sulfur amount of S@ZrO_2/RGO cathode. The cycling performances of the S@ZrO_2/RGO and the S@RGO cathodes are presented in **Fig. 4c**, at a current rate of 0.5 C. Apparently, the S@ZrO_2/RGO cathode exhibited a more stable cycling performance than that of S@RGO. Although S@RGO cathode achieved higher initial capacity, it decreased rapidly to 492.5 mAh g^{-1} after 100 cycles, only about 50% retention. Whereas the S@ZrO_2/RGO cathode has high capacity retention of ~80%, maintaining 663.5 mAh g^{-1} after 100 cycles with a high coulombic efficiency about 97%. In the configuration of S@RGO cathode, the active materials are likely to aggregate on the surface of RGO due to its low pore volume. Hence, during the charge-discharge process, the soluble polysulfide intermediate could easily detach from the electrode to the electrolyte and lead to capacity declining. In contrast, the adding layer of ZrO_2 nanoparticles protects most of the active material from lossing into the electrolyte. Additionally, the mesoporous layer also act as efficient polysulfide reservoir to immobilize the polysulfide and prevent their diffusion to the electrolyte, which could minimize the shuttling effect, as well as sustain an excellent cycle stability.

Rate capability of the S@ZrO_2/RGO cathode was studied by repeated charge-discharge tests conducted at increasing current densities from 0.1 C to 1.5 C, and the results are showed in **Fig. 4d**. As the current rate increases, the capacity of the S@ZrO_2/RGO composite decreased slowly from the reversible 905.5 mAh g^{-1} at 0.2 C to 684.9, 597 and 512 mAh g^{-1} at 0.5 C, 1 C, and 1.5 C, respectively. Notably, reversible capacity of 660 and 807.6 mAh g^{-1} were obtained when the current was switched back to 0.5 C and 0.2 C. S@ZrO_2/RGO shows a really good electrochemical performance.

Aiming to examine the stability of the S@ZrO_2/RGO electrodes after discharge-charge process, further analysis was

performed on the cycled electrodes. The distribution of sulfur in ZrO_2/RGO matrix after cycled was examined by elemental mapping and EDS analysis, presented in Supporting Information **Fig. S5(a-e)**. Most of the sulfur is still confined in the ZrO_2/RGO composite, demonstrating a well-maintained state of the electrode. Furthermore, the electrochemical property was evaluated by electrochemical impedance spectroscopy (EIS) (**Fig. S6**). The semicircle in the high-frequency region corresponds to the charge-transfer process through the electrode/electrolyte interface[24]. The smaller charge-transfer resistance indicates a lower electron-transfer resistance. It is notable that, after it was fully discharge to 1.5 V at the rate of 0.2 mV/s for 5 cycles, the charge-transfer resistance of S@ZrO_2/RGO is 16.4 Ω, much lower than 74.2 Ω that of the S@RGO composite. This is demonstrating that the ZrO_2/RGO composite is an excellent conductive matrix for high performance lithium-sulfur battery. Because the uniform ZrO_2 nanoparticles are in intimate contact with RGO sheets, realizing a porous layered structure for well distribution of sulfur, therefore, improve the conductivity of the entire electrode.

In summary, we have designed and prepared a novel kind of layered porous ZrO_2/RGO framework material. Sulfur is infusion into its homogeneous pores. When evaluated as the cathode material for high performance lithium-sulfur battery, the S@ZrO_2/RGO cathode exhibit a superior electrochemical performance compared with the S@RGO composites. This can be well attributed to the well-designed layered porous architecture. Firstly, the ZrO_2/RGO hybrid provides a high specific surface and large pore volume matrix for sulfur impregnation. Secondly, the porous layers of ZrO_2 nanoparticles function as stable sorption reagent for polysulfide.

Acknowledgements

This work was supported by National Key Project on Basic Research (Grant no. 2011CB935904), the National Natural Science Foundation of China (Grant no.21171163, 91127020), and the NSF for Distinguished Young Scholars of Fujian Province (Grant no. 2013J06006).

Notes and references

[a]*State Key Laboratory of Structural Chemistry, Fujian Institute of Research on the Structure of Matter, Chinese Academy of Sciences, Fuzhou 350002, China. Tel./Fax: 86-591-83792835. E-mail: guanlh@fjirsm.ac.cn.*
[b]*Key Laboratory of Design and Assembly of Functional Nanostructures, Chinese Academy of Sciences， Fuzhou 350002, China*

† Electronic Supplementary Information (ESI) available: [details of any supplementary information available should be included here]. See DOI: 10.1039/b000000x/

‡ Footnotes should appear here. These might include comments relevant to but not central to the matter under discussion, limited experimental and spectral data, and crystallographic data.

1. N. S. Choi, Z. Chen, S. A. Freunberger, X. Ji, Y. K. Sun, K. Amine, G. Yushin, L. F. Nazar, J. Cho and P. G. Bruce, *Angew. Chem., Int. Ed.,* 2012, **51**, 9994-10024.
2. P. G. Bruce, S. A. Freunberger, L. J. Hardwick and J. M. Tarascon, *Nat. Mater.,* 2012, **11**, 19-29.
3. D. Bresser, S. Passerini and B. Scrosati, *Chem. Commun.,* 2013, **49**, 10545-10562.
4. Y.-X. Yin, S. Xin, Y.-G. Guo and L.-J. Wan, *Angew. Chem., Int. Ed.,* 2013, **52**, 13186-13200.
5. G. Zhou, D.-W. Wang, F. Li, P.-X. Hou, L. Yin, C. Liu, G. Q. Lu, I. R. Gentle and H.-M. Cheng, *Energ. Environ. Sci.,* 2012, **5,** 8901-8906.
6. N. Jayaprakash, J. Shen, S. S. Moganty, A. Corona and L. A. Archer, *Angew. Chem., Int. Ed.,* 2011, **50**, 5904-5908.
7. H. Kim, J. T. Lee, D.-C. Lee, A. Magasinski, W.-i. Cho and G. Yushin, *Adv. Energy Mater.,* 2013, **3**, 1308-1315.
8. W. Zhou, Y. Yu, H. Chen, F. J. DiSalvo and H. D. Abruna, *J. Am. Chem. Soc.,* 2013, **135**, 16736-16743.
9. X. Ji, K. T. Lee and L. F. Nazar, *Nat. Mater.,* 2009, **8,** 500-506.
10. R. Chen, T. Zhao, J. Lu, F. Wu, L. Li, J. Chen, G. Tan, Y. Ye and K. Amine, *Nano Lett.,* 2013, **13**, 4642-4649.
11. X. Yang, L. Zhang, F. Zhang, Y. Huang and Y. Chen, *ACS Nano,* 2014, **8**, 5208-5215.
12. X. Ji, S. Evers, R. Black and L. F. Nazar, *Nat. Commun.,* 2011, **2**, 325.
13. L. Yin, J. Wang, F. Lin, J. Yang and Y. Nuli, *Energ. Environ. Sci.,* 2012, **5,** 6966-6972.
14. K. T. Lee, R. Black, T. Yim, X. Ji and L. F. Nazar, *Adv. Energy Mater.,* 2012, **2**, 1490-1496.
15. X. Han, Y. Xu, X. Chen, Y.-C. Chen, N. Weadock, J. Wan, H. Zhu, Y. Liu, H. Li, G. Rubloff, C. Wang and L. Hu, *Nano Energy,* 2013, **2,** 1197-1206.
16. B. Ding, G. Xu, L. Shen, P. Nie, P. Hu, H. Dou and X. Zhang, *J. Mater. Chem. A,* 2013, **1,** 14280.
17. M. Yu, W. Yuan, C. Li, J.-D. Hong and G. Shi, *J. Mater. Chem. A,* 2014, **2**, 7360-7366.
18. K. H. Kim, Y.-S. Jun, J. A. Gerbec, K. A. See, G. D. Stucky and H.-T. Jung, *Carbon,* 2014, **69**, 543-551.
19. J. Cho, Y. J. Kim, T. J. Kim and B. Park, *Angew. Chem., Int. Ed.,* 2001, **40**, 3371-3373.
20. S. M. Lee, S. H. Oh, J. P. Ahn, W. I. Cho and H. Jang, *J. Power Sources,* 2006, **159**, 1334-1339.
21. H. Liu, G. X. Wang, D. Wexler, J. Z. Wang and H. K. Liu, *Electrochem. Commun.,* 2008, **10**, 165-169.
22. J. Hassoun and B. Scrosati, *Adv. Mater.,* 2010, **22**, 5198-5201.
23. S. J. Rettig and J. Trotter, *Acta Crystallogr., Sect. C,* 1987, **43**, 2260-2262.
24. L. Yuan, X. Qiu, L. Chen and W. Zhu, *J. Power Sources,* 2009, **189**, 127-132.

